

## Research Papers

## Comparative Modelling Studies of 400 MHz ST-X Quartz SAW Delay Lines for Potential Gas Sensing Applications

Venkatesan THIRUMAL<sup>(1)</sup>, Banupriya RAJU<sup>(2)</sup>, Pandiyarajan GANDHI<sup>(1)</sup>, Haresh M. PANDYA<sup>(1)</sup><sup>(1)</sup> Department of Physics

Chikkanna Government Arts College

Tiruppur – 641602, Tamilnadu, India; e-mail: haresh.pandya@rediffmail.com

<sup>(2)</sup> Department of Physics

Gobi Arts and Science College

Gobichettipalayam, Tamilnadu, India

(received April 1, 2017; accepted November 28, 2017)

Surface Acoustic Wave (SAW) devices like delay lines, filters, resonators etc., are nowadays extensively used as principal solid state components in many electronic applications and chemical vapour sensors. To bring out the best from these SAW devices, computational design and modelling are resorted too. The present paper proposes the modelling of 400 MHz ST-X Quartz based SAW delay line, by three models namely, Impulse Response Model (IRM), Crossed-field Equivalent Circuit Model (ECM) and Coupling-of-Modes (COM) model. MATLAB<sup>®</sup> is employed as a computational tool to model the experimental output of the SAW device. A comparative discussion of the modelled device results is also provided.

**Keywords:** SAW delay line; impulse response model; equivalent circuit model; COM model; SAW sensors.

## 1. Introduction

Presently, sensing technology makes a prolific use of a wide variety of physical, chemical and biological sensors for investigating and monitoring solid (KANNAN *et al.*, 2004), liquid (BUI *et al.*, 2015; 2016) and gaseous phases in many applications (LIU *et al.*, 2011; STAPLES, VISWANATHAN, 2005). Among these sensors, the gas sensors play a crucial role in domestic and industrial fronts and also helps to predict the presence of organic volatile compounds like pollutants, explosive materials and drugs (LIU *et al.*, 2012). The gas sensors can be measured precisely using conventional analytical methods, such as gas chromatography and gas chromatography based mass spectrometry (PENZA, CASSANO, 2003). However, these methods are expensive and not portable besides giving a relatively complex behaviour and slow performance. To override these gaps, the electronic nose (E-nose) sensor (SINGH *et al.*, 2014), is perhaps the only device which gives timely warning and shows promising characteristics for the detection of toxic and harmful gases (RAJ *et al.*, 2013) simultaneously with desired accuracy (RAJ *et al.*, 2017). These sensors employing the Surface Acoustic Wave (SAW) technology are highly

sensitive to surface perturbations allowing even sub-ppb level detection (RAJ *et al.*, 2010). The advantages of these SAW sensors include compact size, speed, reliability, accuracy, low cost, real time measurement, high sensitivity, room temperature detection and wireless sensing in inaccessible areas (SINGH *et al.*, 2014).

SAW delay line devices are the basic portion of SAW sensors (FILIPIAK *et al.*, 2012). The principal solid state components of SAW sensors consist in measuring time delay changes, frequency changes due to SAW propagation on the piezoelectric substrate between two IDTs, which is caused by device parameters that are being measured (FILIPIAK *et al.*, 2012).

A typical SAW device consists of a piezoelectric substrate with interdigital transducers (IDTs) (WHITE, 1967). The IDT is bidirectional as SAWs are propagating both to the left and to the right from the IDT (WHITE, VOLTMER, 1965). As the electrical signals are applied to input IDT, it converts the applied electrical signals to mechanical signals (Surface Acoustic Waves) which then propagate through the piezoelectric substrate (SHARMA *et al.*, 2014). The mechanical signals are finally detected from the output IDT. The travel length between two IDT is called as delay length (VENKATESAN, PANDYA, 2013). Fig-

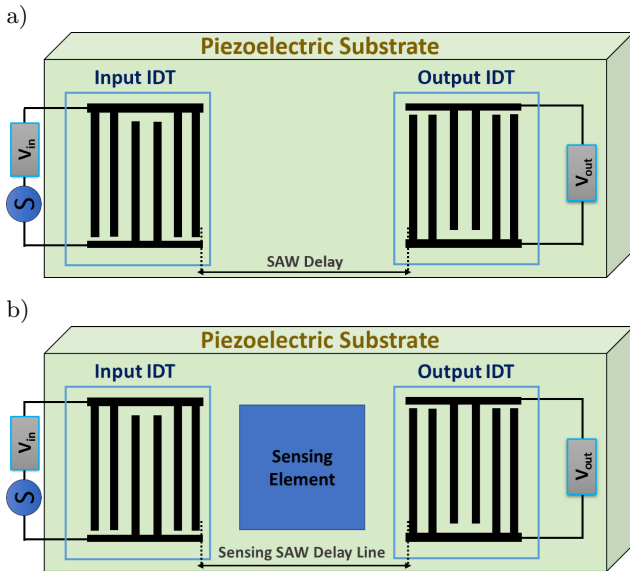


Fig. 1. a) Surface acoustic wave device (basic SAW delay line), b) SAW delay line sensor.

ure 1a shows the basic schematic diagram of the SAW delay line sensor without sensing element and Fig. 1b shows the SAW delay line sensor with sensing element. Only this SAW delay line will be exposed to the harsh environment by sensing the gas/vapour adsorption.

The interdigital transducer consists of a series of interleaved electrodes made of a metal film deposited on a piezoelectric substrate as shown in Fig. 1. It is well known that double or split electrodes are needed whenever they are allowed by fabrication constraints, subsequently they nearly eliminate mass/electrical loading (MEL) reflections and allow the designer to achieve high acoustic return loss (at a sacrifice in insertion loss) by varying the load resistance (SMITH, 1974). Also, triple transit echo (TTE) effect is involved in this study because TTE is due to multiple SAW reflections between bidirectional input and output IDTs which recombine and result in additional voltages at the output IDT creating ripples in the SAW passband (LU *et al.*, 2014). Therefore, those spurious responses to be avoided by designing IDTs with split electrode geometry (BRISTOL *et al.*, 1972) so that multiple reflections from the IDTs would then destructively combine to give a resultant which is minimum at the center frequency.

SAW devices are usually modelled to aid in their design and development to cater to customized needs of industry (HARESH *et al.*, 2013). Modelling techniques, which are usually adopted, need to provide fast and highly accurate results from a device designer's point of view. Modelled results obtained computationally also provide a bridge of understanding between modelled parameters and actual device performance in varied situations (WILSON, ATKINSON, 2009a; MENDES *et al.*, 2012). Typically, modelling of a SAW device and its experimental response pro-

vides a wealth of information on the physics of the SAW device and its optimal device design parameters like center frequency ( $f_0$ ), piezoelectric substrate, SAW velocity ( $v_s$ ), electromechanical coupling coefficient ( $K^2$ ), number of finger pairs ( $N_p$ ), Interdigital Transducer (IDT) geometry, metallization of IDT ( $\eta$ ), aperture of IDT ( $W$ ), spacing between two adjacent finger ( $D$ ), load and source resistance ( $R_L$  &  $R_S$ ). In the present modelling study, effects of parameters like IDT geometry and number of electrode pairs on the SAW device, bandwidth and insertion loss are studied (BANUPRIYA *et al.*, 2014; 2016; VENKATESAN *et al.*, 2015) for the presence of straightforward responses in the SAW sensors.

Various models are presently being utilized to study the function and operation of a SAW device so as to help in its design and development. Initial models like the Delta Function Model (TANCRELL, HOLLAND, 1971) provide basic and rapid insight on device performance and are based on signal theory analysis. A later model in this category is called the Impulse Response Model (HARTMANN *et al.*, 1973; MALOCHA, 1996), and has been chosen as one of the models in the present paper to study the SAW device response. Later advanced models based on network theory were also developed which were complex, comprehensive and required description of the electro-acoustic interaction between the IDT and the substrate. These models could predict more details of device performance with high accuracy as well as highlight factors that restricted their performance. Of these, the Crossed-Field Equivalent Circuit Model (ECM) (SMITH *et al.*, 1969; 1972; SMITH, PEDLER, 1975) and the Coupling of Modes (COM) Model (PIERCE, 1954) have also been selected in the present paper.

The modus operandi adopted in the present research study is to generate a software algorithm code in MATLAB<sup>®</sup> to simulate a 400 MHz, ST-X Quartz based SAW delay line. The MATLAB<sup>®</sup> code simulates the performance of a SAW delay line with a provision for change in parameters wherever and whenever necessary. Modelled device parameters are input, analyzed and wherever possible graphically represented. The whole purpose of this simulation exercise is to model the SAW delay line for improved device performance and subsequently compare the results obtained from the three selected models namely, Impulse Response (IR) Model, Equivalent Circuit (EC) Model and Coupling of Modes (COM) Model.

## 2. Theoretical analysis

### 2.1. Impulse response model

HARTMANN *et al.* (1973) first developed the impulse response model for the simplest way of understanding the Physics and dynamics of SAW devices.

The analysis and design of SAW transducers by an impulse response description has been reviewed by several authors (VENKATESAN, PANDYA 2013; BANUPRIYA *et al.*, 2014). The impulse response method was used as the starting point for modelling the SAW delay line. This model is effective only for transducers where at least one of the two IDTs has a constant aperture ( $W$ ) or finger overlap. It calculates the device performance from the main parameters like admittance, impedance, frequency response, insertion loss and bandwidth obtained from the modelling process.

Figure 2 represents the mason equivalent circuit for both the IDTs of a SAW delay line (SMITH *et al.*, 1972; WILSON, ATKINSON, 2009b). This diagram represents both the IDTs of a SAW delay line with their equivalent circuit,  $C_T$  represents the total capacitance of the IDTs, and  $B_a(f)$  and  $G_a(f)$  their susceptance and conductance respectively. Source voltage  $V_s$ , the source impedance  $Z_s$  and the load impedance  $Z_l$  (equivalent to  $R_g$ ), which are excluded in the model, are also displayed in Fig. 2. Both the load and input resistance are assumed to be  $50 \Omega$ . The frequency response of the SAW delay line is the ratio of the voltages  $V_2$  over  $V_1$  and is given by (VENKATESAN, PANDYA, 2013),

$$H(f) = 20 \log \left[ \left[ 4K^2 C_s W f_0 N_P^2 \left( \frac{\sin(X)}{X} \right)^2 e^{-j \left( \frac{N_P + D}{f_0} \right)} \right] \right], \quad (1)$$

where  $K^2$  is coupling coefficient,  $W$  is the aperture or finger overlap in the IDT,  $C_s$  is the static capacitance of substrate,  $N_P$  is the number of IDT finger pairs ( $= M = N$ ),  $f_0$  is center frequency, and  $D$  is the delay length in wavelengths between the IDTs. The value of  $X$  in the above equation is  $N_P \pi \left( \frac{f - f_0}{f_0} \right)$ , where  $f$  is the synchronous frequency at any instant of time  $t$ .

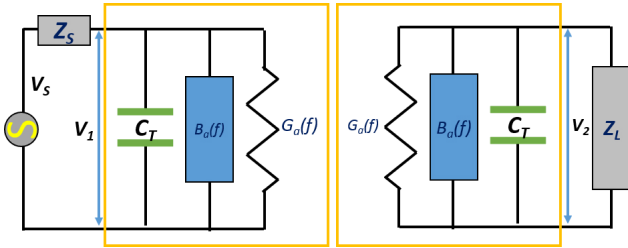


Fig. 2. Mason equivalent circuit for impulse response model (WILSON, ATKINSON, 2009).

The Insertion loss is

$$IL(f) = -10 \log \left[ \frac{2G_a(f)R_g}{(1 + G_a(f)R_g)^2 + a^*} \right], \quad (2)$$

where

$$a^* = (R_g(2\pi f C_t + B_a(f)))^2,$$

$C_t$  is total capacitance,  $G_a(f)$  is susceptance,  $B_a(f)$  is conductance, and  $R_g$  is impedance (HARESH *et al.*, 2013).

## 2.2. Crossed-field Equivalent Circuit Model (ECM)

In the EC model, the electric field distribution under the IDT electrodes is assumed to be normal to the piezoelectric surface, similar to the electric field distribution in a parallel plate capacitor as shown in Fig. 3 (SMITH *et al.*, 1969). The EC model is obtained by small modification of the mason equivalent circuit (SMITH *et al.*, 1972).

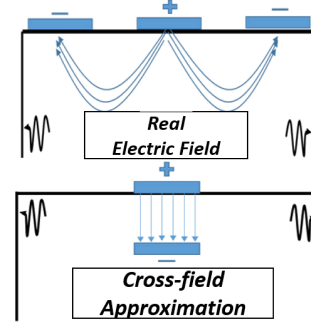


Fig. 3. Electric field direction in crossed-field EC model (SMITH *et al.*, 1969).

The frequency response  $H(f)$ , admittance  $3 \times 3$  matrix of device  $\mathbf{Y}$ , and the Effective Transmission Loss (ETL), can be derived from the potential applied to the electrodes by using the following relations.

In the equivalent circuit model, admittance  $\mathbf{Y}$  is determined by (CAMPBELL, 1989) and given below,

$$\mathbf{Y} = \begin{bmatrix} Y_{11} & Y_{12} & Y_{13} \\ Y_{21} & Y_{22} & Y_{23} \\ Y_{31} & Y_{32} & Y_{33} \end{bmatrix}. \quad (3)$$

The transfer function  $H(f)$  by input voltage ( $V_{in}$ ) and output voltage ( $V_{out}$ ) is

$$H(f) = \frac{V_{out}}{V_{in}} = \left\{ \frac{Y_{ab} R_L}{b^*} \right\}, \quad (4)$$

where

$$b^* = [(1 + Y_{aa} R_s) + (1 + Y_{bb} R_l) - Y_{ab}^2 R_s R_l].$$

Effective transmission loss (ETL) in decibels (MATH- EWS, 1977) is given by

$$ETL = 20 \log_{10} \left| \frac{c^*}{2R_l Y_{ab}} \right|, \quad (5)$$

where

$$c^* = [(1 + Y_{aa} R_s) + (1 + Y_{bb} R_l) - Y_{ab}^2 R_s R_l] \sqrt{R_l / R_s},$$

$Y_{aa}$  is input admittance,  $Y_{bb}$  is output admittance and  $Y_{ab}$  is transfer admittance;  $R_s$  and  $R_l$  are source and load resistance.

### 2.3. Coupling of Modes (COM) model

The COM model of the IDT (PIERCE, 1954) is modelled by deriving and solving the COM equations which considered the voltage and resistance of the IDT finger electrodes simultaneously (ZHANG *et al.*, 2006). Figure 4 represents the COM coordinates of a typical IDT structure. In this model, only the wave amplitudes ( $\omega_i^+$ ;  $\omega_i^-$ ) and variation of acoustic properties as well as the interaction of waves in the propagation direction are taken into account (PLESSKY, KOSKELA, 2000). The forward and backward SAWs in the IDT are combined together. If the period of any periodic structure in the path of acoustic waves  $p$  is close to half of the wavelength ( $p = \lambda/2$ ), these waves travelling in either directions get reflected constructively and destructively at two discrete frequencies forming a stop-band. The spatially varying current  $I(x)$  is induced by the propagation of SAW (HAUS, HUANG, 1991).

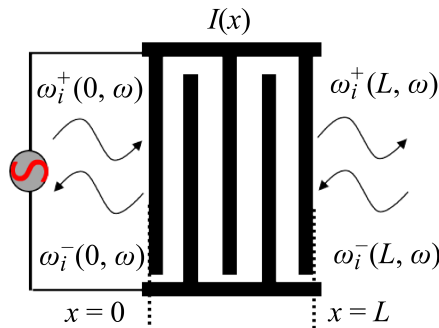


Fig. 4. COM coordinates of an IDT.

The modus operandi here is to model a SAW device by calculating the transfer function by applying appropriate boundary conditions. In Fig. 1a, SAW delay line can be divided into 3 segments namely, input IDT, output IDT and the gap in-between them. These segments are represented by their transmission matrices

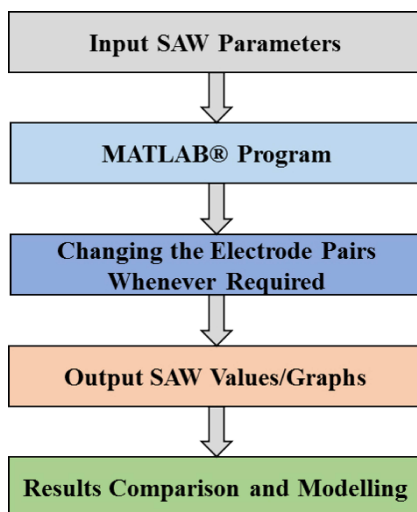


Fig. 5. Flow chart of modelling strategy.

and then finally the total device transmission matrix  $M$  is written as

$$M = T_1 D_2 T_3. \quad (6)$$

The scattering matrix of an IDT is represented as (CROSS, SCHMIDT, 1977)

$$[T_1] = [T_3] = [T] = \begin{bmatrix} s(1+t_0)e^{j\theta_t} & -st_0 & t_{13} \\ st_0 & s(1-t_0)e^{-j\theta_t} & t_{13}e^{-j\theta_t} \\ st_{13} & -st_{13}e^{-j\theta_t} & t_{33} \end{bmatrix}, \quad (7)$$

where  $s = (-1)^{N_t}$ ,  $\theta_t = N_t \Lambda \delta$ ,  $s$  is symmetry parameter and is dependent on  $N_t$ , the number of IDT electrodes,  $\Lambda$  is the grating period and  $\delta$  is the frequency detuning parameter. In Fig. 4,  $a_i$  and  $b_i$  represent complex electrical input and output strengths at the  $i$ -th port. The overall device response can be obtained from the electrical output voltage  $V_{\text{out}}$ , which is written as

$$V_{\text{out}} = b_3 = [\tau'_3] * [W_3], \quad (8)$$

where  $[\tau'_3]$  called the output coupling column matrix and  $[W_3]$  represents the wave amplitudes to the right of IDT2 whose value is calculated to be

$$[W_3] = \begin{bmatrix} \omega_3^+ \\ 0 \end{bmatrix}, \quad (9)$$

where  $\omega_3^+ = \frac{-a_1 \tau_3(1,1)}{M(1,1)}$  is obtained by solving the radiation conductance by applying the boundary conditions  $\omega_0^+ = \omega_0^- = 0$  and  $b_1 = a_3 = 0$  and  $\tau_3$  is column matrix relating to input coupling matrix.

The transmission matrix for the gap  $D_2$  can be represented by  $2 \times 2$  matrix and given as

$$[D_2] = \begin{bmatrix} e^{j\beta d} & 0 \\ 0 & e^{-j\beta d} \end{bmatrix}, \quad (10)$$

where  $\beta = 2\pi/\lambda$  is called the phase constant for SAW delay line sensor without sensing element,  $d$  is the gap length and  $\lambda$  is the wavelength at the given frequency  $f_0$ .

### 3. Modelling strategy

The various steps adapted for modelling of SAW delay line devices are highlighted as follows:

- 1) Best substrate for efficient SAW propagation is selected (the substrate properties are shown in Table 1 (VENKATESAN, PANDYA, 2013)) for modelling purposes. In the present study, ST-X Quartz piezoelectric substrate was selected, as one of its important parameters, namely the Temperature Coefficient of Delay (TCD) which stands for the stability of a SAW device against changes in temperature (CAMPBELL, 1989), is nearly zero.

Table 1. Input parameters for modelling of SAW delay line device.

| S. No | Parameter (symbol)                          | Values                    |
|-------|---|---------------------------|
| 1.    | Coupling coefficient, $K^2$                 | 0.0016 (ST-X Quartz)      |
| 2.    | SAW velocity, $V_S$                         | 3158 m/s                  |
| 3.    | Static capacitance, $C_s$                   | $0.55 \cdot 10^{-10}$ F/m |
| 4.    | Operating frequency, $f_0$                  | 400 MHz                   |
| 5.    | IDT geometry                                | single and split geometry |
| 6.    | Number of finger pairs, $N_P$               | 30 and 40 pairs           |
| 7.    | Load and source resistance, $R_L$ and $R_S$ | 50 $\Omega$               |

- 2) IDT material chosen is aluminium (Al) because aluminium serves as an inert metal as well as a good adhesive (WHITE, 1967).
- 3)  $\lambda$  is the wave periodicity or the uniform electrode spacing of the IDT structure. It also corresponds to the IDT center wavelength at the SAW center frequency of operation  $f_0$ .
- 4) The metallization ratio ( $\eta = a/b$ ) value is 0.5, which is a very important parameter in the design. It means that the spacing between the two adjacent or width of the electrode metal (a) and the combined metal cum finger spacing (b). Also,  $h/\lambda$  is called the film thickness ratio where  $h$  is the IDT metallization thickness 2000 Å or 0.2  $\mu\text{m}$  (SMITH, PEDLER, 1975).
- 5) The input parameters for SAW delay line device modelling according to all three models are depicted in Table 1.
- 6) The modelling strategy adapted is shown in Fig. 5.

#### 4. Modelling of SAW sensor characterization

In SAW delay line sensor, the delay path can be divided into 3 segments namely, the length of gap in-between input IDT and sensing element [ $D_{s1}$ ], the length of sensing element [ $D_{s2}$ ] and the length of gap in-between sensing element and output IDT [ $D_{s3}$ ], and are shown in Fig. 6.

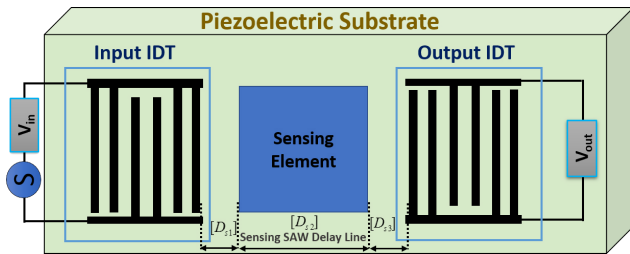


Fig. 6. Sensing SAW delay line.

The phase constant of the SAW device with the sensing element,  $\beta_1 = 2\pi f \frac{D_{s1}}{V_s} + 2\pi f \frac{D_{s2}}{V_m} + 2\pi f \frac{D_{s3}}{V_s}$  at the given frequency  $f$ ,  $V_m$  is the phase velocity of SAW in the sensing element. Therefore, the phase

difference between the SAW travelling in two different paths can be calculated by the adsorption of the gas/vapour (MALIK *et al.*, 2011; HEJCZYK *et al.*, 2015). The usual technique adopted by SAW sensors is to measure shifts in the wave propagation velocity of the surface wave as a function of changes in center frequency of the device or insertion loss. The perturbations to SAW velocity are assumed to be small. However, they can be attributed to many factors such as temperature ( $T$ ), electric field ( $E$ ), stiffness ( $c$ ), density ( $\rho$ ), shear elastic modulus ( $\mu$ ), electrical conductivity ( $\sigma$ ), mass ( $m$ ), permittivity ( $\epsilon$ ), pressure ( $p$ ) and viscosity ( $\eta$ ), each representing a potential sensor response (RICCO, MARTIN, 1991) and if linearly combined can be written as (RICCO, MARTIN, 1991)

$$\frac{\Delta f}{f_0} = \frac{\Delta v}{v_0} \approx \frac{1}{v_0} \left( \frac{\delta v}{\delta T} \Delta T + \frac{\delta v}{\delta \epsilon} \Delta \epsilon + \frac{\delta v}{\delta E} \Delta E + \frac{\delta v}{\delta \sigma} \Delta \sigma + \frac{\delta v}{\delta m} \Delta m + \frac{\delta v}{\delta p} \Delta p + \dots \right). \quad (11)$$

Therefore, the resultant fractional change in center frequency due to mass loading effect by polymer coating film in SAW sensor is given by WOHLTJEN (1984)

$$\Delta f = (k_1 + k_2) f^2 h \rho, \quad (12)$$

where the quantity  $h\rho$  is simply the mass per unit area of the coating film. Small variations in either  $h$  or  $\rho$  will cause a corresponding variation in the device operating frequency. Also, the magnitude of the frequency shift ( $\Delta f$ ) produced by changes in mass per unit area (i.e. sensitivity) is highly frequency dependent. For example, the thickness of the polymer coating film is  $h = 2 \cdot 10^{-6}$  m and the density is  $\rho = 1000$  kg/m<sup>3</sup>, for ST-X quartz SAW sensor ( $k_1 = -9.33 \cdot 10^{-8}$ ,  $k_2 = -4.16 \cdot 10^{-8}$  (m<sup>2</sup>·s)/kg) operating at 400 MHz. Therefore, the simplified theoretically predicts a frequency shift ( $\Delta f$ ) is  $-43.168$  MHz.

#### 5. Results

As per the modelling strategy outlined, MATLAB® program codes were developed for a 400 MHz, ST-X Quartz based SAW delay line device

based on the fundamental physics equations of the three models. In each of these modelling studies, two SAW delay line devices with 30 and 40 IDT finger pairs each, in both Single and Double IDT geometry were modelled. From the modelled responses of the SAW delay line device, the Insertion Loss and 3 dB Bandwidth are graphically obtained and the modelled output values are compared.

Figure 7 shows the 400 MHz SAW delay line responses from above listed model results for 30 and 40 electrode pairs of single and double geometry IDTs, respectively. Thus, these three modelled output values are found successful and the values corresponding to insertion loss and 3 dB bandwidth are represented in Table 2 and Table 3, respectively.

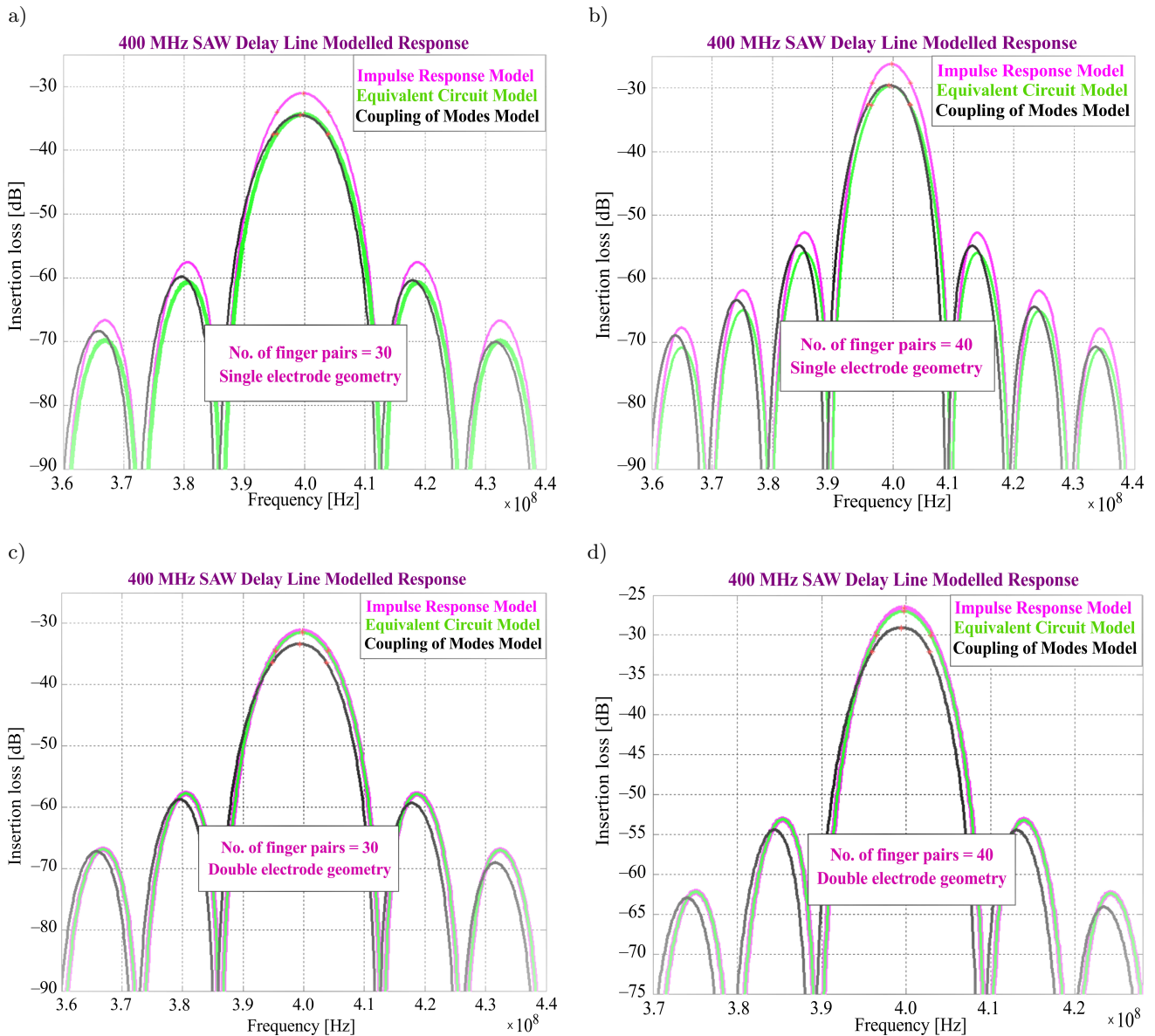


Fig. 7. Modelled Insertion Loss: a) 30 finger pairs, single electrode geometry; b) 40 finger pairs, single electrode geometry; c) 30 finger pairs, double electrode geometry; d) 40 finger pairs, double electrode geometry.

Table 2. Comparison of insertion loss.

| $N_p$ | Insertion loss [dB]       |          |           |                           |          |           |
|-------|---------------------------|----------|-----------|---------------------------|----------|-----------|
|       | Single electrode geometry |          |           | Double electrode geometry |          |           |
|       | IR Model                  | EC Model | COM Model | IR Model                  | EC Model | COM Model |
| 30    | -31.0437                  | -34.3810 | -34.5219  | -31.2868                  | -31.5197 | -33.3934  |
| 40    | -26.2278                  | -29.6813 | -29.5727  | -26.6404                  | -27.0332 | -29.1008  |

Table 3. Comparison of 3 dB bandwidth.

| $N_p$ | 3 dB bandwidth [MHz]      |          |           |                           |          |           |
|-------|---------------------------|----------|-----------|---------------------------|----------|-----------|
|       | Single electrode geometry |          |           | Double electrode geometry |          |           |
|       | IR Model                  | EC Model | COM Model | IR Model                  | EC Model | COM Model |
| 30    | 8.4863                    | 8.5778   | 8.9431    | 8.4865                    | 8.5521   | 8.9524    |
| 40    | 6.3675                    | 6.4815   | 6.8383    | 6.3683                    | 6.4525   | 6.8468    |

## 6. Conclusion

400 MHz ST-X Quartz SAW delay line devices were modelled and the results obtained from Impulse Response model, Crossed-field Equivalent Circuit model and Coupling of Modes (COM) model were compared by employing MATLAB as a simulation tool. The computationally modelled device responses provide simple and effective insights into the physics of SAW devices and their operation via the models adopted in the study. The modelling study points to the fact that for single electrode geometry devices, results of EC and COM models match each other closely (insertion loss  $\sim 0.1409$  dB for 30 electrode pairs and  $\sim 0.1092$  dB for 40 electrode pairs) whereas for double electrode geometry devices, IR and EC models show closer results (Insertion loss  $\sim 0.2329$  dB for 30 electrode pairs and  $\sim 0.3928$  dB for 40 electrode pairs). Thus, IR and EC models are better suited for double electrode IDT devices as the responses in these devices are realized due to an increase in the area of metallization, mass loading effect and total capacitance. It can also have concluded that EC and COM models are suitable for single electrode IDT devices due to the presence of a large unmetallized area, lesser mass loading effect and low capacitance. Such results pave way for actual modelling and simulation of these devices as SAW sensors. Validation of the modelled results will be undertaken in the future experimentally.

## References

- BANUPRIYA R., VENKATESAN T., PANDIYARAJAN G., PANDYA H.M. (2014), *SAW devices – a comprehensive review*, Journal of Environmental Nanotechnology, **3**, 3, 106–115, doi: 10.13074/jent.2014.09.143101.
- BANUPRIYA R., VENKATESAN T., PANDYA H.M. (2016), *A comparison of surface acoustic wave (SAW) delay line modelling techniques for sensor applications*, Journal of Environmental Nanotechnology, **5**, 2, 42–47, doi: 10.13074/jent.2016.06.162193.
- BRISTOL T.W., JONES W.R., SNOW P.B., SMITH W.R. (1972), *Applications of double electrodes in acoustic surface wave device design*, [in:] 1972 IEEE Ultrasonics Symposium, pp. 343–345, doi: 10.1109/ULT-SYM.1972.196097.
- BUI T.H., DUC T.B., DUC T.C. (2015), *Microfluidic injector simulation with FSAW sensor for 3-D integration*, IEEE Transactions on Instrumentation and Measurement, **64**, 4, 849–856, doi: 10.1109/TIM.2014.2366975.
- BUI T., MORANA B., SCHOLTES T., DUC T.C., SARRO P.M. (2016), *A mixing surface acoustic wave device for liquid sensing applications: design, simulation, and analysis*, Journal of Applied Physics, **120**, 7, 1–10, doi: 10.1063/1.4961214.
- CAMPBELL C.K. (1989), *Applications of surface acoustic and shallow bulk acoustic wave devices*, Proceedings of the IEEE, **77**, 10, 1453–1484, doi: 10.1109/5.40664.
- CAMPBELL C. (1989), *Surface acoustic wave devices and their signal processing applications*, London: Academic Press.
- CROSS P.S., SCHMIDT R.V. (1977), *Coupled surface-acoustic-wave resonators*, Bell System Technical Journal, **56**, 8, 1447–1482, doi: 10.1002/j.1538-7305.1977.tb00571.x.
- FILIPIAK J., SOLARZ L., STECZKO G. (2012), *SAW delay line for vibration sensors*, Acta Physica Polonica A, **122**, 5, 808–813, doi: 10.12693/APhysPolA.122.808.
- HARTMANN C.S., BELL D.T., ROSENFELD R.C. (1973), *Impulse model design of acoustic surface-wave filters*, IEEE Transactions on Microwave Theory and Techniques, **21**, 4, 162–175, doi: 10.1109/TMTT.1973.1127967.
- HAUS H.A., HUANG W. (1991), *Coupled-mode theory*, Proceedings of the IEEE, **79**, 10, 1505–1518, doi: 10.1109/5.104225.
- HEJCZYK T., URBAŃCZYK M., PUSTELNY T., JAKUBIK W. (2015), *Numerical and experimental analysis of the response of a SAW structure with  $WO_3$  layers on action of carbon monoxide*, Archives of Acoustics, **40**, 1, 19–24, doi: 10.1515/aoa-2015-0003.
- KANNAN G.K., BHALLA R., KAPOOR J.C., NIMAL A.T., MITTAL U., YADAVA R.D.S. (2004), *Detection of landmine signature using SAW-based polymer-coated chemical sensor*, Defence Science Journal, **54**, 3, 309–315, doi: 10.14429/dsj.54.2044.
- LIU J., WANG W., LI S., LIU M., HE S. (2011), *Advances in SAW gas sensors based on the condensate-adsorption effect*, Sensors, **11**, 12, 11871–11884, doi: 10.3390/s111211871.

15. LIU X., CHENG S., LIU H., HU S., ZHANG D., NING H. (2012), *A survey on gas sensing technology*, *Sensors*, **12**, 12, 9635–9665, doi: 10.3390/s120709635.
16. LU X., MOUTHAN K., SOON Y.T. (2014), *Wide-band bandpass filters with SAW-filter-like selectivity using chip SAW resonators*, *IEEE Transactions on Microwave Theory and Techniques*, **62**, 1, 28–36, doi: 10.1109/TMTT.2013.2292041.
17. MALIK A.F., BURHANUDIN Z.A., JEOTI V. (2011), *A flexible polyimide based SAW delay line for corrosion detection*, *National Postgraduate Conference – Energy and Sustainability: Exploring the Innovative Minds, NPC 2011*, doi: 10.1109/NatPC.2011.6136384.
18. MALOCHA D.A. (1996), *Surface acoustic wave design fundamentals*, *Archives of Acoustics*, **21**, 4, 387–398, <http://acoustics.ippt.gov.pl/index.php/aa/article/view/1008>.
19. MATHEWS H. (1977), *Surface wave filters design, construction and use*, New York: John Wiley & Sons.
20. MENDES J.C., FERNANDES M., MUKHERJEE D., SANTOS D.M. (2012), *Simulation of acoustic wave devices using Matlab*, *Przegląd Elektrotechniczny*, **88**, 155–158.
21. PANDYA H.M., SHARMA M.U., NIMAL A.T., RAJESH K.B. (2013), *Impulse modelled response of a 300 MHz ST-quartz SAW device for sensor specific applications*, *Journal of Environmental Nanotechnology*, **2**, 15–21, doi: 10.13074/jent.2013.02.nciset33.
22. PENZA M., CASSANO G. (2003), *Application of principal component analysis and artificial neural networks to recognize the individual VOCs of methanol/2-propanol in a binary mixture by SAW multi-sensor array*, *Sensors and Actuators B: Chemical*, **89**, 3, 269–284. doi: 10.1016/S0925-4005(03)00002-9.
23. PIERCE J.R. (1954), *Coupling of modes of propagation*, *Journal of Applied Physics*, **25**, 2, 179, doi: 10.1063/1.1721599.
24. PLESSKY V., KOSKELA J. (2000), *Coupling-of-modes analysis of SAW devices*, *International Journal of High Speed Electronics and Systems*, **10**, 4, 867–947, doi: 10.1142/S0129156400000684.
25. RAJ V.B., NIMAL A.T., PARMAR Y., SHARMA M.U., SREENIVAS K., GUPTA V. (2010), *Cross-sensitivity and selectivity studies on ZnO surface acoustic wave ammonia sensor*, *Sensors and Actuators B: Chemical*, **147**, 2, 517–524, doi: 10.1016/j.snb.2010.03.079.
26. RAJ V.B., SINGH H., NIMAL A.T., SHARMA M.U., GUPTA V. (2013), *Oxide thin films (ZnO, TeO<sub>2</sub>, SnO<sub>2</sub>, and TiO<sub>2</sub>) based surface acoustic wave (SAW) E-nose for the detection of chemical warfare agents*, *Sensors and Actuators B: Chemical*, **178**, 636–647, doi: 10.1016/j.snb.2012.12.074.
27. RAJ V.B., SINGH H., NIMAL A.T., SHARMA M.U., TOMAR M., GUPTA V. (2017), *Distinct detection of liquor ammonia by ZnO/SAW sensor: study of complete sensing mechanism*, *Sensors and Actuators B: Chemical*, **238**, 83–90, doi: 10.1016/j.snb.2016.07.040.
28. RICCO A.J., MARTIN S.J. (1991), *Thin metal-film characterization and chemical sensors – monitoring electronic conductivity, mass loading and mechanical-properties with surface acoustic-wave devices*, *Thin Solid Films*, **206**, 94–101, doi: 10.1016/0040-6090(91)90399-I.
29. SHARMA M.U., DINESH KUMAR D., KOUL S.K., VENKATESAN T., PANDIYARAJAN G., NIMAL A.T., KUMAR P.R., PANDYA H.M. (2014), *Modelling of SAW devices for gas sensing applications – a comparison*, *Journal of Environmental Nanotechnology*, **3**, 4, 63–66, doi: 110.13074/jent.2014.12.144110.
30. SINGH H., RAJ V.B., KUMAR J, MITTAL U., MISHRA M., NIMAL A.T., SHARMA M.U., GUPTA V. (2014), *Metal oxide SAW E-nose employing PCA and ANN for the identification of binary mixture of DMMP and methanol*, *Sensors and Actuators B: Chemical*, **200**, 147–156, doi: 10.1016/j.snb.2014.04.065.
31. SMITH W.R. (1974), *Experimental distinction between crossed-field and in-line three-port circuit models for interdigital transducers*, *IEEE Transactions on Microwave Theory and Techniques*, **22**, 11, 960–964, doi: 10.1109/TMTT.1974.1128393.
32. SMITH W.R., GERARD H.M., COLLINS J.H., REEDER T.M., SHAW H.J. (1969), *Analysis of interdigital surface wave transducers by use of an equivalent circuit model*, *IEEE Transactions on Microwave Theory and Techniques*, **17**, 11, 856–864, doi: 10.1109/TMTT.1969.1127075.
33. SMITH W.R., GERARD H.M., JONES W.R. (1972), *Analysis and design of dispersive interdigital surface-wave transducers*, *IEEE Transactions on Microwave Theory and Techniques*, **20**, 7, 458–471, doi: 10.1109/TMTT.1972.1127786.
34. SMITH W.R., PEDLER W.F. (1975), *Fundamental and harmonic-frequency circuit-model analysis of interdigital transducers with arbitrary metallization ratios and polarity sequences*, *IEEE Transactions on Microwave Theory and Techniques*, **23**, 11, 853–864, doi: 10.1109/TMTT.1975.1128703.
35. STAPLES E.J., VISWANATHAN S. (2005), *Ultrahigh-speed chromatography and virtual chemical sensors for detecting explosives and chemical warfare agents*, *IEEE Sensors Journal*, **5**, 4, 622–631, doi: 10.1109/JSEN.2005.850990.
36. TANCRELL R.H., HOLLAND M.G. (1971), *Acoustic surface wave filters*, *Proceedings of the IEEE*, **59**, 3, 393–409, doi: 10.1109/PROC.1971.8180.
37. VENKATESAN T., BANUPRIYA R., PANDIYARAJAN G., PANDYA H.M. (2015), *Idealized P-matrix based modelling and computational analysis of SAW delay lines for improved performance in sensors*, *Journal of Environmental Nanotechnology*, **4**, 4, 56–61, doi: 10.13074/jent.2015.12.154170.
38. VENKATESAN T., PANDYA H.M. (2013), *Surface acoustic wave devices and sensors – a short review on*

- design and modelling by impulse response*, Journal of Environmental Nanotechnology, **2**, 3, 81–89, doi: 10.13074/jent.2013.09.132034.
39. WHITE R.M. (1967), *Surface elastic-wave propagation and amplification*, IEEE Transactions on Electron Devices, **14**, 4, 181–189, doi: 10.1109/T-ED.1967.15926.
40. WHITE R.M., VOLTMER F.W. (1965), *Direct piezoelectric coupling to surface elastic waves*, Applied Physics Letters, **7**, 12, 314, doi: 10.1063/1.1754276.
41. WILSON W.C., ATKINSON G.M. (2009a), *A comparison of surface acoustic wave modeling methods*, Micro Devices to Wireless Systems, **7**, 150–150.
42. WILSON W., ATKINSON G. (2009b), *Comparison of transmission line methods for surface acoustic wave modeling*, Sensors & Transducers Journal, **7**, 150–159.
43. WOHLTJEN H. (1984), *Mechanism of operation and design considerations for surface acoustic wave device vapour sensors*, Sensors and Actuators, **5**, 4, 307–325, doi: 10.1016/0250-6874(84)85014-3.
44. ZHANG X., XU Y., ZHAO M., PAN M., FAN Y., ZHANG Z. (2006), *Modeling and simulation of wireless passive pressure sensors based on surface acoustic wave resonators*, 2006 8th International Conference on Signal Processing, doi: 10.1109/ICOSP.2006.346055.